Density-based Global Sensitivity Analysis of Islanded Microgrid Loadability Considering Distributed Energy Resource Integration

Zhuoxin Lu, Xiaoyuan Xu, Zheng Yan, and Han Wang

***Abstract*—With the proliferation of renewable energy and electric vehicles (EVs), there have been increasing uncertainties in power systems. Identifying the influencing random variables will reduce the effort in uncertainty modeling and improve the controllability of power systems. In this paper, a density-based global sensitivity analysis (GSA) method is proposed to evaluate the influence of uncertainties on islanded microgrids (IMGs). Firstly, the maximum IMG loadability evaluation model is established to assess the distance from the current operation point to the critical operation point. Secondly, the Borgonovo method, which is a density-based GSA method, is used to evaluate the influence of input variables on IMG loadability. Thirdly, to improve GSA efficiency, a modified Kriging model is used to obtain a surrogate model of IMG loadability, and Borgonovo indices are calculated based on the surrogate model. Finally, the proposed method is tested on a 38-bus IMG system. Simulation results are compared with those considering other methods to validate the effectiveness of the proposed method. Energy storage systems are considered to diminish the influence of critical uncertainties on IMG operation.**

***Index Terms*—Islanded microgrids (IMGs), renewable energy, global sensitivity analysis, uncertainty.**

I. Introduction

A microgrid (MG) is a small-scale power system that integrates distributed generation (DG) units and loads. MGs can be operated in the grid-connected or islanded mode. In the grid-connected mode, MG is connected to the utility grid, and its operation is the same as that of active distribution systems. In the islanded mode, there is no reference bus, and the frequency and bus voltage of islanded MGs (IMGs) are regulated by DG units governed by droop characteristics [1]-[4].

IMGs are fed by a small group of capacity-limited DG units. Therefore, the stable operation of IMGs is significantly affected by uncertainties, and IMGs are likely to reach their critical operation points. The maximum loadability of transmission systems is usually used to evaluate its static voltage stability margin. Different from that of transmission systems, the maximum loadability of IMGs describes the distance from the current state to the critical state considering the operation characteristic of droop-controlled DG units. Reference [5] used the continuation power flow (CPF) to evaluate IMG loadability. Reference [6] considered the static voltage and small-signal stability constraints in IMG loadability evaluation. Reference [7] established a bi-objective optimal power flow (OPF) model for maximizing loadability and minimizing operating costs, in which probability models were used to describe uncertain renewable energy generation output power and load demands. In [8], CPF combined with the two-point estimate method was proposed to obtain the probability distribution of IMG loadability.

The maximum loadability is uncertain due to a large number of random variables. Sensitivity analysis (SA) is an effective method to evaluate the influence of random variables on IMG loadability. Local sensitivity analysis (LSA), which is usually based on the derivative of output with respect to input, has been widely used in power system analyses. Different from LSA, GSA is applicable to nonlinear problems. Moreover, it evaluates the influence of random variables considering its whole range of variation [9]. However, the applications of GSA in power systems are much more limited. Recently, [10] used GSA to evaluate the importance of uncertainties for power system small-signal stability. Reference [11] assessed the impact of uncertainties on system frequencies. Reference [12] proposed a GSA method to identify critical variables affecting bus voltages and line flows. Reference [13] used GSA to evaluate the impact of variable renewable energy on power system voltage stability. References [14] and [15] applied GSA to probabilistic power flow problems for analyzing the influence of renewable energy.

Monte Carlo simulation (MCS) is usually used in GSA, but it suffers from heavy computational burden. To improve GSA efficiency, surrogate models are used in place of original problems to calculate global sensitivities (GSs). Reference [16] compared several surrogate methods in multidisciplinary design and optimization problems. Reference [17] used polynomial chaos expansion (PCE) to obtain probabilis-

Manuscript received: September 2, 2018; accepted: June 5, 2019. Date of CrossCheck: June 5, 2019. Date of online publication: October 7, 2019.

This work was supported by National Natural Science Foundation of China (No. 51707115).

Z. Lu, X. Xu (corresponding author), Z. Yan, and H. Wang are with Key Laboratory of Control of Power Transmission and Conversion of Ministry of Education, Shanghai Jiao Tong University, Shanghai, China (e-mail: Zhuoxin_Lu@sjtu.edu.cn; xuxiaoyuan@sjtu.edu.cn; yanz@sjtu.edu.cn; wanghan9894@sjtu.edu.cn).

DOI: 10.35833/MPCE.2018.000580

tic models of IMG loadability. Reference [18] proposed a new surrogate method that combined PCE with Kriging models, which was more accurate than conventional PCE.

In this paper, we propose an efficient GSA method and apply it to evaluate the influence of uncertainties on maximum IMG loadability. Firstly, a stochastic optimization problem is established to evaluate the maximum loadability of IMGs. Then, the Borgonovo method, which is a density-based GSA method, is used to evaluate the influence of uncertainties on IMG loadability. To improve computational efficiency of GSA, PCE combined with Kriging (PCE-Kriging) is utilized to establish surrogate models of IMG loadability, and GSs are calculated based on PCE-Kriging models. Finally, the proposed method is tested on a 38-bus IMG system. The influences of uncertainties, including renewable energy generation outputs and electric vehicle (EV) charging demands, are investigated. Energy storage systems (ESSs) are considered to reduce the variability of IMG loadability.

II. IMG Loadability Evaluation

This section presents the evaluation model of IMG loadability. Firstly, the models of droop-controlled DG units, load demands and ESSs are given. Then, the probability models are designed to describe the variabilities of EV charging demands and renewable energy generation outputs. Finally, an optimization model is established for the evaluation of IMG loadability.

A. Droop-controlled DG

Droop-controlled DG units are responsible for regulating the system frequency and bus voltages of IMGs [19]. Here, the *P-f/Q-V* control strategy is used to describe the behavior of droop-controlled DG units, which is stated as:

$$\begin{cases} P_{Gi} m_{pi} = f_0 - f \\ Q_{Gi} n_{qi} = V_{i0} - V_i \end{cases} \tag{1}$$

where P_{Gi} and Q_{Gi} are the active and reactive power outputs of droop-controlled DG units, respectively; m_{pi} and n_{qi} are the active and reactive power droop gains, respectively; f is the system frequency; V_i is the voltage magnitude of bus i; and f_0 and V_{i0} are the nominal values of f and V_i, respectively.

The output power of DG units follows the droop characteristic before it reaches limits. Beyond the output power limits, the DG unit is transformed to inject constant power at the maximum active or reactive power. Therefore, the behavior of capacity-limited droop-controlled DG units is described as follows [7], [17]:

$$\begin{cases} P_{Gi,ub} - P_{Gi} \ge 0 \\ f_0 - f - P_{Gi} m_{pi} \ge 0 \\ \left(P_{Gi,ub} - P_{Gi}\right)\left(f_0 - f - P_{Gi} m_{pi}\right) = 0 \\ Q_{Gi,ub} - Q_{Gi} \ge 0 \\ V_{i0} - V_i - Q_{Gi} n_{qi} \ge 0 \\ \left(Q_{Gi,ub} - Q_{Gi}\right)\left(V_{i0} - V_i - Q_{Gi} n_{qi}\right) = 0 \end{cases} \tag{2}$$

where $P_{Gi,ub}$ and $Q_{Gi,ub}$ are the maximum active and reactive power outputs of DG units, respectively.

B. Load

The load is a function of system frequency and bus voltage, which is stated as [17]:

$$\begin{cases} P_{Li} = \left(P_{Li0} + \lambda P_{Li0}\right)\left(\dfrac{V_i}{V_{i0}}\right)^{\gamma_{pi}}\left(1 + k_{Pi}\dfrac{f - f_0}{f_0}\right) \\ Q_{Li} = \left(Q_{Li0} + \lambda Q_{Li0}\right)\left(\dfrac{V_i}{V_{i0}}\right)^{\gamma_{qi}}\left(1 + k_{Qi}\dfrac{f - f_0}{f_0}\right) \end{cases} \tag{3}$$

where P_{Li} and Q_{Li} are the active and reactive power of load demands, respectively; P_{Li0} and Q_{Li0} are the active and reactive power of load demands at the current operating point, respectively; γ_{pi} and γ_{qi} are the exponents of loads; k_{Pi} and k_{Qi} are the static frequency characteristic factors; and λ is the IMG loadability, which describes the distance from the current operation point to the critical operation point. In this paper, we use the load demands at the current operation point as the incremental rates. Note that the incremental rates of load demands can also be designed based on actual operating conditions, which may be different for different buses.

C. ESS

Renewable-based DG (RDG) units are equipped with ESSs to reduce the variability of its output power. There are various operation strategies for ESSs. Here, a simple strategy is designed as follows. The maximum state of charge (SOC) and minimum SOC are designed as 100% and 10% of the ESS capacity, respectively. When the output power of RDG units is larger than the charging threshold, ESS is operated in the charging status. When the output power of RDG units is smaller than the discharging threshold, ESS is operated in the discharging status. Considering the maximum charging and discharging power of ESS, its operation strategy is described as:

$$P_{ESS} = \begin{cases} \min\left(P_{\max}, \eta_d P_{mo} - P_{RDG}\right) & P_{RDG} < \eta_d P_{mo} \\ \max\left(-P_{\max}, \eta_c P_{mo} - P_{RDG}\right) & P_{RDG} > \eta_c P_{mo} \end{cases} \tag{4}$$

where P_{ESS} is the charging or discharging power of the ESS; $P_{\max}$ is the maximum charging or discharging power of the ESS; P_{RDG} is the output power of RDG units; P_{mo} is the maximum output power of RDG units; and η_d and η_c are the discharging and charging threshold coefficients, which are set as 20% and 50%, respectively [20], [21].

The SOC of ESS is related to the SOC in the last instant and the charging or discharging power in the current instant, which is described as:

$$SOC_t \cdot E = SOC_{t-1} \cdot E + \left(kP_{charge} - P_{discharge}/k\right)\Delta t \tag{5}$$

where SOC_{t-1} and SOC_t are the states of charging at instants t+1 and t, respectively; E is the maximum capacity of the ESS; k is the charging or discharging efficiency, which is set as 85%; P_{charge} and $P_{discharge}$ are the charging power and discharging power, respectively; and Δt is the time interval, which is set as 10 min.

D. Uncertainty

1) Plug-in hybrid EV (PHEV)

The charging of plug-in PHEVs is an important load de-

mand in MGs. The PHEV charging demand is variable since it is affected by various factors such as the battery capacity, operation status and charging strategy. Here, we use the probability model in [22] to describe the variability of PHEV charging demands. Specifically, the active power of PHEV charging stations is described by a Weibull distribution, and the active power of PHEV charging in residential communities is described by a normal distribution.

2) RDG

The output power of RDG units is affected by weather conditions such as wind speed and solar irradiance. Since parametric models may not accurately describe the probability models of variables, kernel density estimation (KDE) [23] is used to estimate the probability distributions of wind speed and solar irradiance. Let X_1, X_2, …, X_N be historical data; the underlying probability density of the variable x is estimated by:

$$\hat{f}(x)=\frac{1}{Nh}\sum_{i=1}^{N}K\frac{x-X_i}{h} \tag{6}$$

where N is sample size; h is bandwidth; and K is the kernel function. The accuracy of $\hat{f}(x)$ depends on the selection of bandwidth and kernel function. The Gaussian Copula is used in our research, and the Silverman's method [24] is used to estimate the bandwidth.

The active power of wind power and photovoltaic (PV) units are dependent on wind speed and solar irradiance, respectively [25]. The reactive power of wind power units is modeled to maintain the power factor constant. The power factor of PV units is set as 1.

E. Maximum Loadability Assessment Model

The IMG loadability assessment model is stated as the maximization of λ, subject to the power flow constraints (7), droop-controlled DG constraints (8) and boundary constraints (9).

1) Power flow constraints

$$\begin{cases}V_i\sum V_j\left(G_{ij}\cos\theta_{ij}+B_{ij}\sin\theta_{ij}\right)=P_{Gi}+P_{Ri}-P_{Li}\\ V_i\sum V_j\left(G_{ij}\sin\theta_{ij}-B_{ij}\cos\theta_{ij}\right)=Q_{Gi}+Q_{Ri}-Q_{Li}\end{cases} \tag{7}$$

where G_{ij} and B_{ij} are the conductance and susceptance between nodes i and j, respectively; and P_{Ri} and Q_{Ri} are the active and reactive power outputs of RDG units, respectively.

2) Droop-controlled DG constraints

$$\begin{cases}f_0-f-P_{Gi}m_{pi}\ge 0\\ V_0-V_i-Q_{Gi}n_{qi}\ge 0\\ \left(P_{Gi,ub}-P_{Gi}\right)\left(f_0-f-P_{Gi}m_{pi}\right)=0\\ \left(Q_{Gi,ub}-Q_{Gi}\right)\left(V_0-V_i-Q_{Gi}n_{qi}\right)=0\end{cases} \tag{8}$$

3) Boundary constraints

$$\begin{cases}V_{i,lb}\le V_i\le V_{i,ub}\\ P_{Gi,lb}\le P_{Gi}\le P_{Gi,ub}\\ Q_{Gi,lb}\le Q_{Gi}\le Q_{Gi,ub}\\ P_{ij,lb}\le P_{ij}\le P_{ij,ub}\end{cases} \tag{9}$$

where $V_{i,lb}$ and $V_{i,ub}$ are the lower and upper limits of voltage magnitude, respectively; $P_{ij,lb}$ and $P_{ij,ub}$ are the lower and upper limits of active power flow through lines, respectively; and $Q_{ij,lb}$ and $Q_{ij,ub}$ are the lower and upper limits of reactive power flow through lines, respectively.

III. Global Sensitivity Analysis

In this section, we propose a global sensitivity analysis (GSA) method to evaluate the influences of uncertain renewable energy generation outputs and load demands on IMG loadability.

A. Borgonovo Method

The maximization of λ is a nonlinear optimization problem with random variables. The uncertain renewable energy generation outputs and load demands are treated as random input variables, and the maximum IMG loadability is the random output variable. Then, the Borgonovo method, one of the GSA methods, is used to evaluate the influence of input variables on the output variable [10]. The Borgonovo index is defined as:

$$\delta=\frac{1}{2}\int f_{x_i}(x_i)\left(\int\left|f_y(y)-f_{y|x_i}(y)\right|\mathrm{d}y\right)\mathrm{d}x_i \tag{10}$$

where x_i is the random input variable; y is the random output variable; $f_{x_i}(x_i)$ is the probability density of x_i; $f_{y_i}(y_i)$ is the probability density of y; and $f_{y|x_i}(y)$ is the conditional density of y when x_i is a deterministic input.

B. PCE-Kriging Model

MCS can be used to calculate the Borgonovo index, but it suffers from heavy computational burden, which limits its application in practical problems. Here, we first surrogate the output variable using the PCE-Kriging model and then calculate the Borgonovo index based on the surrogate model, which will significantly improve GSA efficiency.

The PCE-Kriging model is stated as:

$$G(\boldsymbol{x})\approx G^{(K)}(\boldsymbol{x})=\boldsymbol{\beta}^{\mathrm{T}}\boldsymbol{\varphi}(\boldsymbol{x})+\sigma^2 Z(\boldsymbol{x}) \tag{11}$$

where $G(\boldsymbol{x})$ is the exact output value with random input variable $\boldsymbol{x}=[x_1, x_2, \ldots, x_n]$; $G^{(K)}(\boldsymbol{x})$ is the PCE-Kriging model output with input variables $\boldsymbol{x}$; $\boldsymbol{\varphi}(\boldsymbol{x})$ is a set of orthogonal polynomials; $\boldsymbol{\beta}$ is the coefficients of polynomials; σ^2 is the constant variance; and $Z(\boldsymbol{x})$ is a Gaussian process (GP) with zero mean and unit variance.

$\boldsymbol{\beta}^{\mathrm{T}}\boldsymbol{\varphi}(\boldsymbol{x})$ is presented as PCE, which is stated as [18]:

$$\boldsymbol{\beta}^{\mathrm{T}}\boldsymbol{\varphi}(\boldsymbol{x})=\sum_{\alpha\in A}m_\alpha\Psi_\alpha(\boldsymbol{x}) \tag{12}$$

where A is the set of sparse polynomial base indices; Ψ_α is the polynomial bases of PCE; and m_α is the coefficients of polynomial bases. The number of polynomial bases significantly increases in high-dimensional problems. The least angle regression method [26] is used to select important bases, thus establishing sparse PCE in the Kriging model.

The autocorrelation function of $Z(\boldsymbol{x})$ describes the dependence between different points of the stochastic process. The Gaussian autocorrelation function is defined as:

$$R=\exp\left(-\sum_{i=1}^{n}\left(\frac{\left|x_{k,i}-x_{l,i}\right|}{\theta_i}\right)^2\right) \tag{13}$$

where $x_{k,i}$ and $x_{l,i}$ are the k^{th} and l^{th} samples of variable x_i, respectively; and θ_i represents the hyperparameters obtained by minimizing the cross-validation error [27].

C. Evaluating Influence of Uncertainty on Loadability

The procedure to evaluate the influence of uncertainties on IMG loadability is given in Fig. 1. Using PCE-Kriging to surrogate maximum loadability and calculating the Borgonovo index using surrogate models are the key steps.

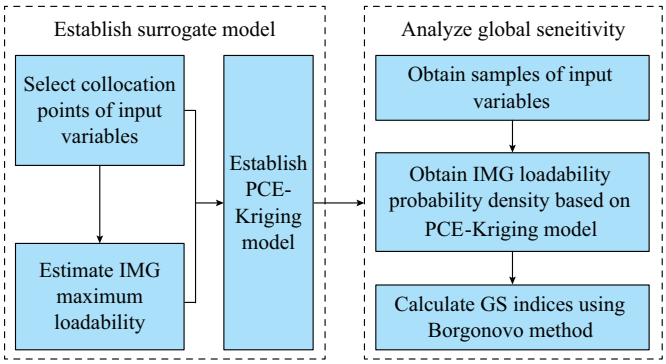

Fig. 1. Flowchart of evaluating influence of uncertainties on IMG loadability.

IV. Case Studies

In this section, the proposed method is tested using a 38-bus IMG system. The variabilities of renewable energy generation outputs and load demands are considered, and the uncertain IMG loadability is evaluated. The accuracy of the PCE-Kriging model for IMG loadability is analyzed, and the influence of uncertainties on IMG loadability is discussed. We use OPTI toolbox to solve the nonlinear optimization problem and use UQLab toolbox to establish PCE-Kriging models [28]. The program is developed using MATLAB on PC with 2.80 GHz CPU and 8.0 GB RAM.

A. System Description

The diagram of the 38-bus IMG system is given in Fig. 2. The feeder parameters and nominal loads are found in [29]. Three droop-controlled DG units, three wind power units and two PV units are allocated to feed the IMG system. The parameters of droop-controlled DG units are given in Table I. PHEV charging stations are connected to buses 25 and 29, and PHEV charging in residential communities is considered at buses 11 and 21. The probability models of PHEV charging demands are given in Table II. In normal distribution model, σ is the standard deviation, μ is the mean value. In Weibull distribution model, c is the scale parameter and k is the shape parameter. The active power of load demands at other buses is described by normal distributions with the standard deviation equal to 20% of the mean. The upper and lower limits of voltage magnitude are defined as 0.95 p.u. and 1.05 p.u., respectively. The upper and lower limits of the system frequency are set as 0.995 p.u. and 1.005 p.u., respectively.

The parameters of RDG units are given in Table III and Table IV. In Table III, v_r is the rated wind speed for wind power units; v_{in} and v_{out} are the cut-in and cut-out wind speeds for wind power units, respectively. In Table IV, S is the area of PV power units; η is the energy conversion efficiency of PV power units. The measured data of wind speed and solar irradiance in Gansu Province, China are used to describe the uncertain outputs of RDG units.

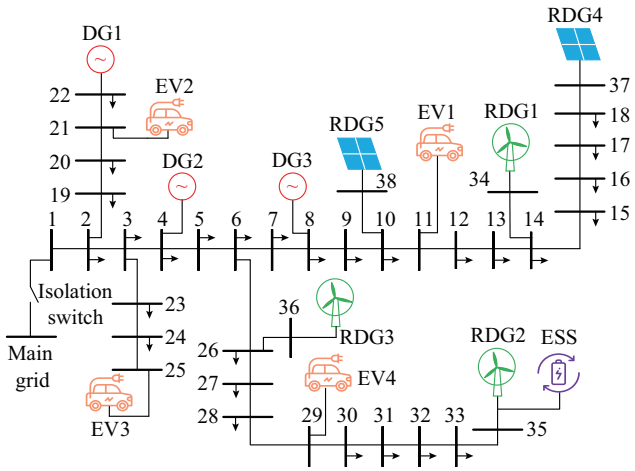

Fig. 2. Diagram of 38-bus IMG system.

TABLE I
Parameters of Droop-Controlled DG Units

Bus	$P_{G,ub}$ (p.u.)	$Q_{G,ub}$ (p.u.)	m_{pi}	n_{qi}	V_0	f_0
4	3.0	1.5	0.000729	0.0000165	1.0009	1.016
8	0.5	1.0	0.004030	0.0617000	1.0008	1.016
22	1.5	1.0	0.001220	0.0321000	1.0009	1.040

TABLE II
Probability Models of PHEV Charging Demand

EV	Bus	Model	Parameter	Mean (MW)
EV1	11	Normal	$\sigma/\mu = 0.15$	0.20
EV2	21	Normal	$\sigma/\mu = 0.15$	0.40
EV3	25	Weibull	$c = 0.19, k = 2.06$	0.17
EV4	29	Weibull	$c = 0.19, k = 2.06$	0.17

TABLE III
Parameters of Wind Power Units

RDG	Bus	Type	v_{in} (m/s)	v_r (m/s)	v_{out} (m/s)	Rated power (MW)	Power factor
RDG1	34	Wind	3.0	15	19	0.70	0.90
RDG2	35	Wind	3.7	13	18	0.83	0.90
RDG3	36	Wind	3.3	14	19	0.80	0.90

TABLE IV
Parameters of PV Units

RDG	Bus	Type	S (m^3)	η (%)	Power factor
RDG4	37	PV	6000	15	1.00
RDG5	38	PV	4000	15	1.00

B. Surrogate Model of IMG Loadability

PCE-Kriging is compared with MCS, Kriging and PCE in obtaining IMG loadability. 1000 samples are used in the four methods, and MCS with a sample size of 10000 is used as the benchmark to test the accuracy of different methods.

Figure 3 shows the probability density functions (PDFs) and cumulative distribution functions (CDFs) of IMG loadability. PCE-Kriging obtains the most accurate IMG loadability, since the probability distribution obtained by PCE-Kriging is nearly the same as that by MCS using 10000 samples. The difference between the probability distributions obtained by Kriging and PCE and that by MCS is relatively larger. Besides, if a small number of samples are used in MCS, for example 1000, it cannot obtain accurate results.

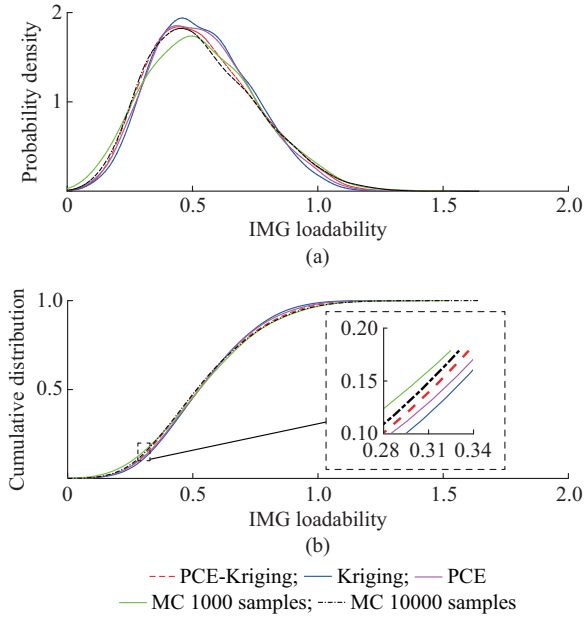

Fig. 3. Probability distributions of IMG loadability obtained by different methods. (a) Probability density comparison. (b) Cumulative distribution comparison.

The computation time of PCE-Kriging and MCS is given in Table V. There are 37 random input variables when the variabilities of RDG outputs and loads are considered. There are 5 random input variables when only the variabilities of RDG outputs are considered. The total computation time of PCE-Kriging is about 10% of the total computation time of MCS.

TABLE V
COMPUTATION TIME OF MCS AND PCE-KRIGING IN OBTAINING PROBABILITY DISTRIBUTIONS OF IMG LOADABILITY

Number of variables	Method	Computation time by IMG loadability evaluation (s)	Computation time of surrogate model training (s)	Total computation time (s)
37	MCS	1470.4	-	1470.4
37	PCE-Kriging	131.7	25.3	157.0
5	MCS	1397.8	-	1397.8
5	PCE-Kriging	128.2	6.4	134.6

MCS costs long computation time in obtaining the accurate IMG loadability probability distribution, since 10000 samples are used and the original optimization problem is solved for each sample. As to PCE-Kriging, although extra time is needed in the model training, it is much more efficient since fewer samples are needed to obtain accurate surrogate models.

C. Global Sensitivity Analysis

We design the following three cases to calculate the GSs of input variables and evaluate the influence of uncertainties on IMG loadability:

1) Case 1: the original IMG system.
2) Case 2: changing the locations of RDG units.
3) Case 3: changing the penetration level of PHEVs.

In Case 1, there are 37 input variables, and the GS of each input variable is calculated using both the Borgonovo method and the Sobol method, which is a popular variance-based GSA method. Six variables with the largest sensitivities are given in Table VI. The rankings of variables obtained by the Borgonovo and Sobol methods are similar, which validates the correctness of the proposed method. According to the table, the wind power at bus 35 is the most influential factor that affects the IMG loadability, followed by the wind power at buses 34, 36 and the load demand at bus 30. The PV power and the load demands of PHEV charging stations also affect the IMG loadability. While the load demands at other buses make a minor influence due to quite small sensitivities.

TABLE VI
GSA RESULTS OF DIFFERENT METHODS

Rank	Sobol	Borgonovo	
		Kriging	PCE-Kriging
1	RDG2	RDG2	RDG2
2	RDG1	RDG1	RDG1
3	RDG3	RDG3	RDG3
4	Load 30	RDG4	Load 30
5	RDG4	Load 30	RDG4
6	EV4	EV4	EV4

In Case 2, the locations of RDG units are given in Table VII. The GSs of input variables in Cases 1 and 2 are given in Fig. 4. The outputs of RDG units make a significant influence on IMG loadability in both Cases 1 and 2. The output of the second wind power unit is still the most influential factor when it is located on a different bus. Therefore, in this system, the variabilities of RDG outputs, rather than the locations of RDG units, mainly determine the influence of RDG on IMG loadability.

TABLE VII
LOCATION OF RDG UNITS

Case	Location of RDG unit				
	RDG1	RDG2	RDG3	RDG4	RDG5
1	34	35	36	37	38
2	24	28	17	16	32

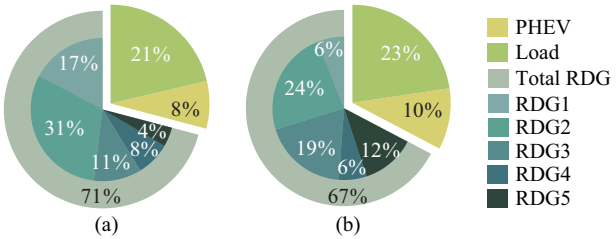

Fig. 4. Sensitivities of uncertainties in Cases 1 and 2. (a) Case 1. (b) Case 2.

In Case 3, the locations and load demands of PHEVs are changed, as shown in Table VIII. Figure 5 shows the GSs of input variables in five scenarios. In Scenario 1, all the loads are described by normal distributions. In Scenario 2, the PHEV charging demands at buses 11, 21, 25, 29 are described by the normal distributions and the Weibull distributions with larger variances. On the one hand, the loads at the four buses have larger sensitivities than those in Scenario 1. On the other hand, their sensitivities are smaller than those of RDG output power, which means that their influence on IMG loadability is smaller. By comparing the result in Scenario 4 with that in Scenario 2, we find that the locations of PHEVs affect their GSs, but the GSs do not change significantly. In Scenarios 3 and 5, the load demand of PHEV charging increases, making them become more influential factors. Therefore, in IMG with a high penetration of PHEVs, the variability of PHEV charging demand makes a significant influence on the system loadability.

TABLE VIII
SCENARIOS IN CASE 3

Scenario	IMG system description
1	Without PHEV charging demand
2	PHEV charging is considered at buses 11, 21, 25, 29
3	PHEV charging demand is two times that in Scenario 2
4	PHEV charging is considered at buses 5, 19, 20, 26
5	PHEV charging demand is two times that in Scenario 4

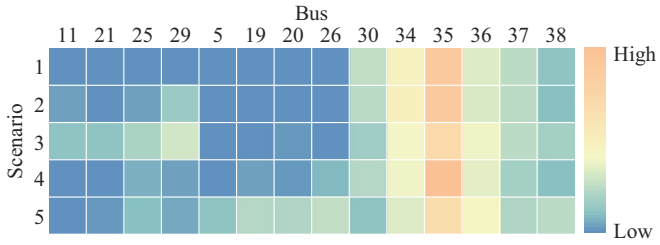

Fig. 5. GSs of input variables for different locations and load demands of PHEVs.

D. Influence of ESS

In this section, ESSs are located according to GSA results. The parameters of ESS are designed as follows: the capacity of each ESS is 3 MW and the initial SOC is set as 60%. The operation strategy of ESSs is given in Section II-C.

Figure 6 gives the time series output power of the unit which combines RDG with ESS (RDG-ESS). Figure 7 gives the probability densities of the output power of RDG and RDG-ESS. As shown in the figure, the variance of the output power of RDG-ESS is smaller than that of RDG.

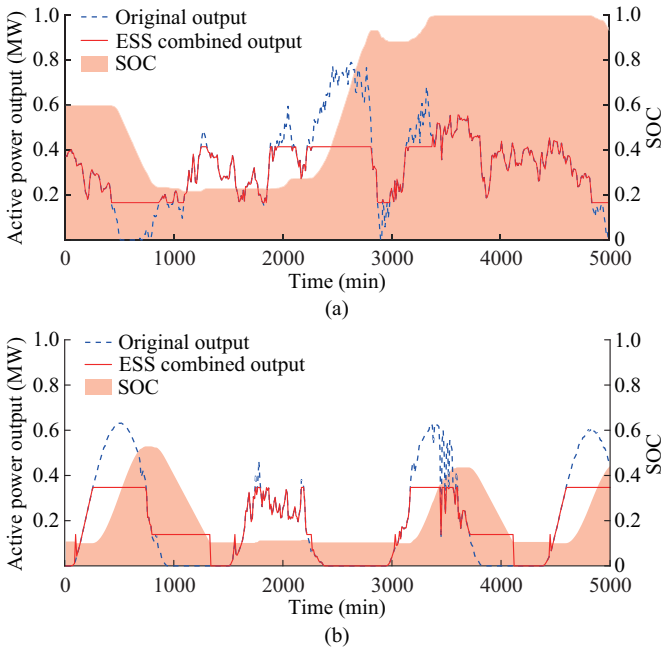

Fig. 6. Time series outputs of RDG and RDG-ESS. (a) Output power of RDG2 (wind power) and RDG2-ESS. (b) Output power of RDG5 (PV) and RDG5-ESS.

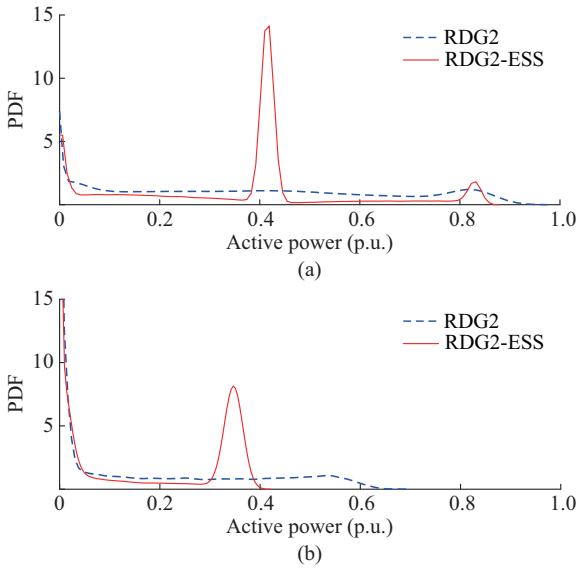

Fig. 7. Probability distributions of output power for RDG units with and without ESSs. (a) Probability densities of output power of RDG2 (wind power) and RDG2-ESS. (b) Probability densities of output power of RDG5 (PV) and RDG5-ESS.

We design the scenarios for different locations of ESSs, as shown in Table IX. The probability densities of IMG loadability are given in Fig. 8, and the means and variances of IMG loadability are given in Table X. The mean of IMG loadability in Scenario 7 is larger than those in other scenarios. The variance of IMG loadability becomes smaller when ESSs are installed. The variances of IMG loadability in Sce-

narios 6 and 7 are much smaller than those in Scenarios 8 and 9. This is because the RDG units which significantly affect IMG loadability are equipped with ESSs. The variability of RDG output decreases, making the variance of IMG loadability smaller. Compared with the results in Scenario 6, the variability of RDG output in Scenario 7 decreases. Thus, the mean of loadability is larger and the variance of loadability is smaller. In Scenario 8, although the variability of the output power of some RDG units also decreases, the probability distribution of loadability almost remains the same since the uncertain power of those units makes a minor influence on the loadability.

TABLE IX
SCENARIOS FOR ESS INSTALLATION

Scenario	IMG system description
6	ESSs are installed at three RDG units with the largest GSs
7	The capacity of each ESS in Scenario 6 is 5 MW
8	ESSs are installed at three RDG units with the smallest GSs
9	ESSs are not installed

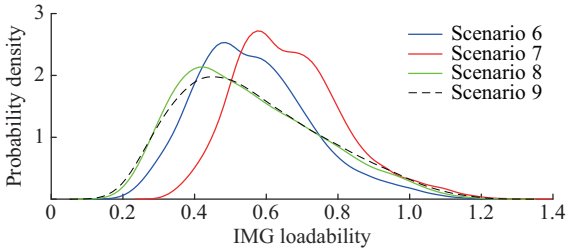

Fig. 8. Probability distributions of IMG loadability in four scenarios.

TABLE X
MEANS AND VARIANCES OF IMG LOADABILITY

Scenario	Mean	Variance
6	0.5637	0.0265
7	0.6655	0.0237
8	0.5534	0.0382
9	0.5629	0.0411

In summary, the variability of IMG maximum loadability decreases when the variability of influential RDG outputs is reduced by ESSs. Therefore, the GSA results provide candidate locations for the optimal locating and sizing of ESSs.

V. CONCLUSION

In this paper, an improved GSA method is proposed to evaluate the influence of variable renewable energy generation outputs and PHEV charging demands on the maximum IMG loadability. The proposed method is tested on a 38-bus IMG system.

Compared with MCS, PCE-Kriging obtains accurate probability distributions of IMG loadability with much fewer samples. The GSs of input random variables are efficiently obtained by combing PCE-Kriging with the Borgonovo method, and they identify critical random variables that affect IMG loadability. Renewable energy generation units with large GSs can be integrated with ESSs to diminish the variability of IMG loadability, thus improving the controllability and stability of IMGs.

REFERENCES

[1] L. Su, J. Zhang, W. Li *et al*., "Study on some key problems and technique related to microgrid," *Power System Protection and Control*, vol. 38, no. 19, pp. 235-239, Oct. 2010.
[2] T. Yu and J. Tong, "Modeling and simulation of the microturbine generation system," *Power System Protection and Control*, vol. 37, no. 3, pp. 27-31, Feb. 2009.
[3] M. Alipour, B. Mohammadi-Ivatloo, and K. Zare, "Stochastic scheduling of renewable and CHP-based microgrids," *IEEE Transactions on Industrial Informatics*, vol. 11, no. 5, pp. 1049-1058, Oct. 2015.
[4] M. Zhang, Q. Xie, L. Li *et al*., "Optimal sizing of energy storage for microgrids considering energy management of electric vehicles," *Proceedings of the CSEE*, vol. 35, no. 18, pp. 4663-4673, Sept. 2015.
[5] G. Diaz, "Maximum loadability of droop regulated microgrids - formulation and analysis," *IET Generation Transmission & Distribution*, vol. 7, no. 2, pp. 175-182, Feb. 2013.
[6] M. M. A. Abdelaziz, E. F. El-Saadany, and R. Seethapathy, "Assessment of droop-controlled islanded microgrid maximum loadability," in *Proceedings of the 2013 IEEE PES General Meeting*, Vancouver, Canada, Jul. 2013, pp. 1-5.
[7] M. M. A. Abdelaziz and E. F. El-Saadany, "Maximum loadability consideration in droop-controlled islanded microgrids optimal power flow," *Electric Power Systems Research*, vol. 106, no. 1, pp.168-179, Jan. 2014.
[8] L. Hu, K. Liu, W. Sheng *et al*., "Fast probabilistic evaluation of static voltage stability in active distribution network considering random output from distributed generations," *Power System Technology*, vol. 38, no. 10, pp. 2766-2771, Oct. 2014.
[9] E. Borgonovo, "A new uncertainty importance measure," *Reliability Engineering & System Safety*, vol. 92, no. 6, pp. 771-784, Jun. 2007.
[10] K. N. Hasan, R. Preece, and J. V. Milanović, "Priority ranking of critical uncertainties affecting small-disturbance stability using sensitivity analysis techniques," *IEEE Transactions on Power Systems*, vol. 32, no. 4, pp. 2629-2639, Oct. 2016.
[11] R. Preece and J. V. Milanović, "Assessing the applicability of uncertainty importance measures for power system studies," *IEEE Transactions on Power Systems*, vol. 31, no. 3, pp. 2076-2084, May 2016.
[12] F. Ni, M. Nijhuis, P. H. Nguyen *et al*., "Variance-based global sensitivity analysis for power systems," *IEEE Transactions on Power Systems*, vol. 33, no. 2, pp. 1670-1682, Mar. 2018.
[13] X. Xu, Z. Yan, M. Shahidehpour *et al*., "Power system voltage stability evaluation considering renewable energy with correlated variabilities," *IEEE Transactions on Power Systems*, vol. 33, no. 3, pp. 3236-3245, May 2018.
[14] K. He, Z. Yan, X. Xu *et al*., "Sobol method based global sensitivity analysis of power flow in islanded microgrid," *Automation of Electric Power Systems*, vol. 42, no. 14, pp. 99-106, Jul. 2018.
[15] H. Wang, Z. Yan, X. Xu *et al*., "Probabilistic power flow calculation of islanded microgrid considering uncertainty of renewable energy,"*Automation of Electric Power Systems*, vol. 42, no.15, pp. 110-117, Aug. 2018.
[16] X. Mu, W. Yao, X. Yu *et al*., "Survey of surrogate models used in MDO," *Chinese Journal of Computational Mechanics*, vol. 22, no. 5, pp. 608-612, Oct. 2005.
[17] X. Xu, Z. Yan, M. Shahidehpour *et al*., "Maximum loadability of islanded microgrids with renewable energy generation," *IEEE Transactions on Smart Grid*, vol. 10, no. 5, pp. 4696-4705, Sept. 2019.
[18] P. Kersaudy, B. Sudret, N. Varsier *et al*., "A new surrogate modeling technique combining kriging and polynomial chaos expansions-application to uncertainty analysis in computational dosimetry," *Journal of Computational Physics*, vol. 286, pp. 103-117, Apr. 2015.
[19] Q. Lei, X. Li, D. Huang *et al*., "Coordinated control for medium voltage DC distribution centers with flexibly interlinked multiple microgrids," *Journal of Modern Power Systems and Clean Energy*, vol. 7, no. 3, pp. 599-611, May 2019.
[20] J. Yang, S. Ouyang, Y. Wu *et al*., "Stochastic power flow of distribution network considering probability model of wind-storage combined systems," *Power System Technology*, vol. 40, no. 1, pp. 234-241, Jan. 2016.
[21] B. Gao, X. Liu, C. Wu *et al*., "Game-theoretic energy management with storage capacity optimization in the smart grids," *Journal of Mo-*

dern Power Systems and Clean Energy, vol. 6, no. 4, pp. 656-667, Jul. 2018.
[22] G. Li and X. Zhang, "Modeling of plug-in hybrid electric vehicle charging demand in probabilistic power flow calculations," *IEEE Transactions on Smart Grid*, vol. 3, no. 1, pp. 492-499, Mar. 2012.
[23] Y. Zhao, X. Zhang, and J. Zhou, "Load modeling utilizing nonparametric and multivariate kernel density estimation in bulk power system reliability evaluation," *Proceedings of the CSEE*, vol. 29, no. 31, pp. 27-33, Nov. 2009.
[24] B. W. Silverman, *Density Stimation for Statistics and Data Analysis*, London: Chapman and Hall, 1986.
[25] Z. Pan, J. Liu, and T. Hou, "Probabilistic evaluation of voltage stability for islanded microgrids with droop-controlled and intermittent distributed generations considering correlation," *Proceedings of the CSEE*, vol. 38, no. 4, pp. 1065-1074, Feb. 2018.
[26] R. Schöbi, S. Marelli, and B. Sudret, "UQLab user manual – PC-Kriging," Report UQLab-V1.0-109, Chair of Risk, Safety & Uncertainty Quantification, ETH Zurich, 2017.
[27] G. Blatman and B. Sudret, "Adaptive sparse polynomial chaos expansion based on least angle regression," *Journal of Computational Physics*, vol. 230, no. 6, pp. 2345-2367, Mar. 2011.
[28] S. Marelli and B. Sudret, "UQLab: a framework for uncertainty quantification in MATLAB," in *Proceedings of 2nd International Conference on Vulnerability, Risk Analysis and Management (ICVRAM2014)*, Liverpool, United Kingdom, Jul. 2014, pp. 2554-2563.
[29] M. E. Baran and F. Wu, "Network reconfiguration in distribution systems for loss reduction and load balancing," *IEEE Transactions on Power Delivery*, vol. 4, no. 2, pp. 1401-1407, Apr. 1989.

Zhuoxin Lu received B.S degree in Electrical Engineering, Chongqing University, Chongqing, China, in 2017. She is currently working toward the Ph. D. degree at the Department of Electrical Engineering, Shanghai Jiao Tong University, Shanghai, China. Her research interests include microgrids operation and planning.

Xiaoyuan Xu received the B.S. and Ph.D. degrees in electrical engineering from Shanghai Jiao Tong University, Shanghai, China, in 2010 and 2016, respectively. He was a visiting scholar with the Robert W. Galvin Center for Electricity Innovation, Illinois Institute of Technology, Chicago, USA, from 2017 to 2018. He is currently an Assistant Professor with Shanghai Jiao Tong University, Shanghai, China. His research interests include power system uncertainty quantification and power system optimization.

Zheng Yan received the B.S. degree from Shanghai Jiao Tong University, Shanghai, China, in 1984, and the M.S. and Ph.D. degrees from Tsinghua University, Beijing, China, in 1987 and 1991, respectively, all in electrical engineering. He is currently a professor of Electrical Engineering with Shanghai Jiao Tong University. His current research interests include application of optimization theory to power systems, power markets, and dynamic security assessment.

Han Wang received the B.S. degree from the College of Electrical Engineering, Zhejiang University, Hangzhou, China, in 2015. He is currently working toward the Ph.D. degree at the Department of Electrical Engineering, Shanghai Jiao Tong University, Shanghai, China. His research interests include power system uncertainty quantification and microgrid control.